Veterinary Microbiology xxx (2015) xxx–xxx

Contents lists available at ScienceDirect

Veterinary Microbiology

journal homepage: www.elsevier.com/locate/vetmic

Structural characterisation of the virulence-associated protein VapG from the horse pathogen *Rhodococcus equi*

Tebekeme Okoko [a,1,2], Elena V. Blagova [b,1], Jean L. Whittingham [b,*], Lynn G. Dover [a], Anthony J. Wilkinson [b]

[a] *Department of Applied Sciences, Faculty of Health and Life Sciences, Northumbria University, Newcastle upon Tyne NE1 8ST, UK*
[b] *Structural Biology Laboratory, Department of Chemistry, University of York, Heslington, York YO10 5DD, UK*

ARTICLE INFO

Article history:
Received 8 January 2015
Received in revised form 30 January 2015
Accepted 31 January 2015

Keywords:
Virulence-associated protein
Rhodococcus equi
Protein Structure
VapG
VapA

ABSTRACT

Virulence and host range in *Rhodococcus equi* depends on the variable pathogenicity island of their virulence plasmids. Notable gene products are a family of small secreted virulence-associated proteins (Vaps) that are critical to intramacrophagic proliferation. Equine-adapted strains, which cause severe pyogranulomatous pneumonia in foals, produce a cell-associated VapA that is necessary for virulence, alongside five other secreted homologues. In the absence of biochemical insight, attention has turned to the structures of these proteins to develop a functional hypothesis. Recent studies have described crystal structures for VapD and a truncate of the VapA orthologue of porcine-adapted strains, VapB. Here, we crystallised the full-length VapG and determined its structure by molecular replacement. Electron density corresponding to the N-terminal domain was not visible suggesting that it is disordered. The protein core adopted a compact elliptical, anti-parallel β-barrel fold with β1–β2–β3–β8–β5–β6–β7–β4 topology decorated by a single peripheral α-helix unique to this family. The high glycine content of the protein allows close packing of secondary structural elements. Topologically, the surface has no indentations that indicate a nexus for molecular interactions. The distribution of polar and apolar groups on the surface of VapG is markedly uneven. One-third of the surface is dominated by exposed apolar side-chains, with no ionisable and only four polar side-chains exposed, giving rise to an expansive flat hydrophobic surface. Other surface regions are more polar, especially on or near the α-helix and a belt around the centre of the β-barrel. Possible functional significance of these recent structures is discussed.

1. Introduction

Rhodococcus equi is a ubiquitous, soil bacterium which has evolved into an opportunistic pathogen through the acquisition of an 80 kbp virulence plasmid. Pathogenic *R. equi* infect different domesticated animal hosts (pigs, sheep and cattle) but are most frequently associated with bronchopneumonial disease in very young foals. It is also an emerging human pathogen, affecting immuno-compromised individuals. In foals, disease is transmitted through inhalation of contaminated dust particles, leading to severe lung infection which eventually spreads to the gut and other areas (Meijer and Prescott, 2004; Vázquez-Boland et al., 2013). Excretion of contaminated faeces completes the infection cycle. Clinical manifestations of *R. equi* lung infection include bronchitis and pulmonary lesions (Prescott, 1991), and in the absence of treatment mortality rates are in the region of 80% (Muscatello et al., 2007). Thus, *R. equi* represents a major threat to foal health

* Corresponding author. Tel.: +44 1904 328270.
E-mail address: jean.whittingham@york.ac.uk (J.L. Whittingham).
[1] These authors contributed equally to the study.
[2] Current address at: Department of Biochemistry, Niger Delta University, Amassama, Wilberforce Island, Bayelsa State, Nigeria.

http://dx.doi.org/10.1016/j.vetmic.2015.01.027
0378-1135/

worldwide and has a significant economic impact on the horse breeding industry. Current treatments for *R. equi* infections involve combination drug therapies with rifampin and macrolides such as clarithromycin (Giguère et al., 2011). These treatments can be protracted and expensive, and are not always successful. Furthermore, antibiotic resistant strains are emerging (Andersen et al., 1997; Asoh et al., 2003). While vaccine trials are on-going and making headway (Hooper-McGrevy et al., 2005; Dawson et al., 2010; Whitehead et al., 2012), there are still no commercially available vaccines, and research investigations are now focussing on the mechanism of pathogenicity induced by *R. equi* in order to provide insights which may ultimately lead to better treatments for infection.

R. equi is a Gram-positive coccobacillus with a lipid-rich cell envelope characteristic of the mycolata, a group of acid-fast actinomycetes that includes *Mycobacterium, Corynebacterium* and *Nocardia* species. It metabolises a wide range of organic and inorganic compounds and thrives on the mixture of organic compounds found in animal manure. Virulent *R. equi* enter alveolar macrophages by receptor-mediated phagocytosis and survive and proliferate in phagosomes. The bacterium has the ability to halt phagosome maturation prior to the late endocytic stage, thereby protecting it from normal bacteriocidal factors and allowing it to proliferate (Fernandez-Mora et al., 2005). Virulence of *R. equi* strains is strictly associated with the possession of an ~80 kbp plasmid (Takai et al., 1991b; Tkachuk-Saad and Prescott,

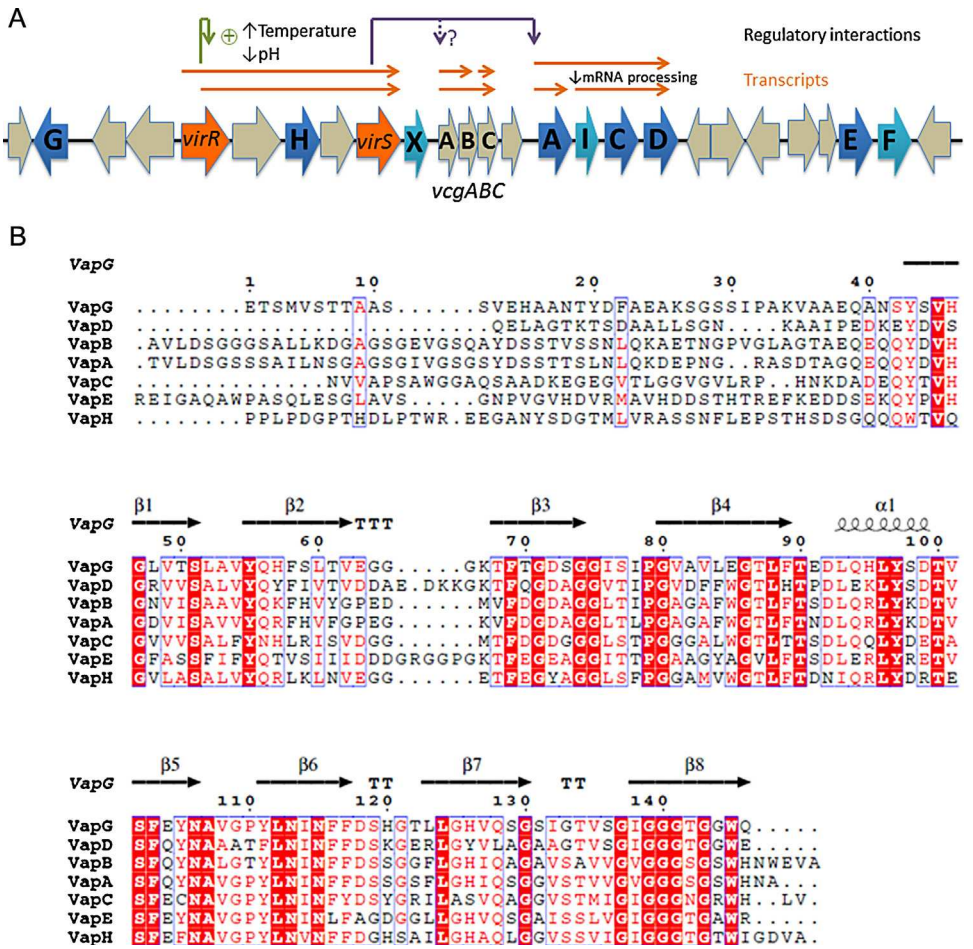

Fig. 1. The virulence genes/proteins of *R. equi*. (A) The 21.3 kb pathogenicity island region of the equine type *R. equi* plasmid pVAPA1037. The genes encoding the homologous virulence associated proteins Vaps A, C, D, E, G, H are shown in blue with a one letter label. The pseudogenes *vapF*, *vapI* and *vapX* are shown in turquoise. The genes encoding the transcriptional regulators *virR* (a LysR type transcriptional regulator) and *virS* (an orphan two-component system response regulator) are coloured in orange. Expression of *vapA* appears to be controlled indirectly by VirR in response to temperatures above 30 °C and acidic pH by production of VirS (green arrow) (Russell et al., 2004), which is required for transcription of the *vapAIC(orfAB)D* operon (purple arrow) (Kakuda et al., 2014); the small uncharacterised ORFs (*orfAB*) that lie between *vapC* and *vapD* are not shown for clarity. The promoter associated with the *vcgABC* operon (uncharacterised *vap* co-expressed genes) shares homology with the *vapA* promoter (Miranda-CasoLuengo et al., 2011) suggesting that a similar mode of regulation may operate. Observed transcripts are related as orange arrows (Byrne et al., 2007, 2008; Kakuda et al., 2014; Miranda-CasoLuengo et al., 2011). (B) Comparison of the amino acid sequences of the Vap proteins of the *R. equi* horse virulence plasmid together with VapB form the porcine virulence plasmid. The sequences were aligned in CLUSTALW (Thompson et al., 1994) and displayed together with the secondary structure elements of VapG using the programme ESPRIPT (Robert and Gouet, 2014). Invariant residues in the alignment are shown in white type on a red background; conserved residues are in blue boxes (For interpretation of the colour information in this figure legend, the reader is referred to the web version of the article.).

Please cite this article in press as: Okoko, T., et al., Structural characterisation of the virulence-associated protein VapG from the horse pathogen *Rhodococcus equi*. Vet. Microbiol. (2015), http://dx.doi.org/10.1016/j.vetmic.2015.01.027

1991). Plasmid-cured strains do not proliferate in macrophages, are cleared in murine models of infection, and are avirulent in foals (Hondalus and Mosser, 1994; Wada et al., 1997; Giguère et al., 1999). The virulence plasmid harbours a pathogenicity island (Fig. 1A) containing 26 coding sequences including that for the virulence-associated protein A (VapA). VapA is an ~20 kDa immunodominant protein present in clinical isolates of infected foals (Takai et al., 1991a,b; Tan et al., 1995). A strain of *R. equi* with a *vapA* deletion mutation was shown to be unable to grow in macrophages and to be incapable of establishing infection in mice pointing to an essential role in virulence (Jain et al., 2003). However, plasmid-encoded factors other than VapA are needed for virulence since expression of wild type levels of VapA in otherwise virulent, plasmid-cured strains of *R. equi* does not restore virulence in mice or foals (Giguère et al., 1999). Similarly, in plasmid pathogenicity island-deleted strains of *R. equi*, constitutive expression of *vapA* could delay clearance of the pathogen from mice but it did not restore virulence (Coulson et al., 2010). Thus *vapA* is necessary but not sufficient for virulence and other pathogenicity island-encoded factors are required.

Also encoded on the pathogenicity island are a set of virulence-associated proteins highly homologous to VapA; VapC, VapD, VapE, VapG, and VapH (Fig. 1A). In addition, there are three pseudogenes *vapF*, *vapI* and *vapX* which are not thought to code for functional proteins since they harbour substantial truncations and/or frameshifts. The role of these additional *vap* genes and whether they encode proteins with overlapping or redundant functions is not established. The available evidence indicates that these genes are not essential for virulence, at least in mice, since a mutant deleted for *vapA, -C, -D, -E* is complemented by *vapA* expressed in *trans* (Jain et al., 2003). The *vap* genes are induced by elevated temperature, starvation of various metals, and low pH, conditions likely to be encountered in the macrophage (Benoit et al., 2001; Ren and Prescott, 2003). *vapA* expression is dependent on two pathogenicity island factors, *virR*, which encodes a LysR type transcriptional regulator and *virS* (*orf8*) which encodes an orphan two-component system response regulator (Fig. 1A) (Ren and Prescott, 2003; Russell et al., 2004). Each of the *vap* genes encodes a secretion signal peptide consistent with the translocation of their gene products to the outside of the cell where many have been detected by immunoblotting of *R. equi* culture supernatants (Byrne et al., 2001). By contrast, VapA appears to be retained on the bacterial cell surface (Takai et al., 1992).

In order to provide a framework for a new set of studies to investigate the critical function(s) of VapA and its role in *R. equi* virulence, we and others have sought to determine its three-dimensional structure. However, crystals of VapA have proved elusive and efforts were directed towards homologous Vap proteins. The crystal structures of two Vap proteins, VapB whose gene resides on a plasmid present in *R. equi* isolates from pigs (Geerds et al., 2014) and VapD (Whittingham et al., 2014) have been determined. An alignment of the sequences of the six plasmid-encoded Vap proteins from horse isolates of *R. equi* together with VapB from pig isolates is presented in Fig. 1B. The structures revealed that the highly conserved C-terminal residues form an eight-stranded β-barrel. In the case of VapD, circular dichroism as well as crystallographic data indicated that the N-terminal region of the protein, whose sequence is poorly conserved across the Vap family, is intrinsically disordered. Here, we are concerned with a third virulence-associated protein VapG. *vapG* expression is known to be highly up-regulated in *R. equi* infected macrophages and in the lungs of infected foals. However, deletion mutagenesis showed VapG to be dispensible for growth of the pathogen in macrophages and *in vivo* in mice (Coulson et al., 2010). In this work, we present the crystal structure of VapG and compare its structure to those of VapB and VapD. The results are discussed in terms of possible functions of the Vap proteins.

2. Materials and methods

2.1. Protein production and purification

VapG was cloned as a commercial service by Eurofins Operon in pET23b. Native *R. equi* sequence was used and fused directly with restriction sites for *Nde*I (5′, with the ATG of the restriction site representing the start codon) and *Eco*RI (3′, directly after the last codon) to form pET23-mat*vapG*.

Transformants of *Escherichia coli* BL21 (DE3) carrying pET23-*vapG* were grown overnight in 10 ml LB broth supplemented with 100 μg ml^{-1} ampicillin at 37 °C with shaking at 200 rpm. This overnight preculture was used to inoculate 1 l of Terrific broth (100 μg ml^{-1} ampicillin) and grown at 37 °C to an OD_{600} of 0.5–0.7 at 180 rpm, 37 °C. The culture was cooled to 16 °C and recombinant gene expression was induced by the addition of 1 mM IPTG; cultures were held at 16 °C overnight before harvesting by centrifugation at 2880 × *g* for 10 min at 4 °C. Pelleted cells were re-suspended to 10 ml/g in 0.02 M Tris–HCl (pH 7.4, containing 0.5 M NaCl, 0.03 M imidazole) and lysed by exposing resuspended cells (in 5 ml aliquots) to 6 cycles of 10 s sonication/10 s cooling with amplitude setting at 10 μ using a MSE Soniprep 150 ultrasonic disintegrator. The lysate was clarified by centrifugation at 27,000 × *g* for 30 min at 4 °C.

Recombinant protein was purified from the clarified lysate via a two-step process using Immobilised Metal Affinity Chromatography (IMAC) on Ni^{2+}-charged Chelating Sepharose Fast Flow resin (GE healthcare Life Sciences) followed by anion-exchange chromatography on HiTrap Q HP. Firstly, the IMAC column (10 ml bed volume) was equilibrated with 200 ml of 0.02 M Tris–HCl (pH 7.4) containing 0.03 M imidazole, 0.5 M NaCl (otherwise known as equilibration buffer) at a flow rate of 5 ml/min (for 20 min). The clarified lysate was loaded onto the column at a flow rate of 2 ml/min and washed with the equilibration buffer at a flow rate of 4 ml/min for 25 min. Elution of bound protein was effected via an linear gradient if imidazole concentration (from 0.03 to 0.5 M) at a flow rate of 4 ml/min. Eluate was collected in 4 ml fractions. The composition of each fraction was analysed on SDS-PAGE to identify those containing VapG.

Please cite this article in press as: Okoko, T., et al., Structural characterisation of the virulence-associated protein VapG from the horse pathogen *Rhodococcus equi*. Vet. Microbiol. (2015), http://dx.doi.org/10.1016/j.vetmic.2015.01.027

Fractions containing VapG were pooled and concentrated to about 0.5 ml by centrifuging at 2880 × *g*, 4 °C using a 10 kDa Vivaspin 20 Centrifugal Concentrator (Sartorius Stedim Biotech, France). This process was repeated three times with 20 ml of ice-cold 0.02 M Tris–HCl (pH 8.0) to remove imidazole and NaCl. After the final concentration, the sample was diluted to a final volume of 20 ml in the same buffer and subjected to anion exchange chromatography on a 5 ml bed volume HiTrap Q HP column equilibrated with 0.02 M Tris–HCl (pH 8.0) at a flow rate of 5 ml/min. The VapG-enriched sample was applied at a flow rate of 2 ml/min and eluted with 0.02 M Tris–HCl, 1 M NaCl (pH 8.0) at a flow rate of 4 ml/min in a linear gradient using 0.02 M Tris–HCl (pH 8.0) as the diluent.

2.2. Size-exclusion chromatography with multi-angle laser light scattering (SEC-MALLS)

For the determination of the oligomeric state of VapG, the protein was analysed by SEC-MALLS. Samples of protein at concentrations of 4 mg/ml were loaded onto a Superdex S75 10/300 gel-filtration column equilibrated at 0.5 ml min^{-1} with a mobile phase consisting of 50 mM Tris–HCl pH 8.0, 150 mM NaCl. The eluate was passed through an SPD20A UV–vis detector, a Wyatt Dawn HELEOS-II 18-angle light-scattering detector and a Wyatt Optilab rEX refractive index monitor with the system driven by a Shimadzu HPLC system comprising an LC-20AD pump. The data were processed and molecular masses were calculated using the Astra V software (Wyatt) as described previously (Colledge et al., 2011).

2.3. Protein crystallisation, data collection, structure solution and refinement

Crystals were obtained using a protein solution consisting of VapG at 30 mg ml^{-1} in 10 mM Tris–HCl (pH 7.5), 10 mM NaCl. The crystals grew at 18 °C by hanging drop vapour diffusion against a reservoir solution containing 0.3 M potassium chloride, 20% PEG 3350, originating from the Peg/Ion screen (Hampton Research). A crystal of approximate dimensions 400 μm × 400 μm × 400 μm was vitrified in cryoprotectant solution (30% glycerol, 70% reservoir) and X-ray diffraction data were collected at 100 K at the Diamond Light Source experimental station I02. Data were integrated using XDS (Kabsch, 2010) and scaled/merged with Aimless (Evans, 2011). The structure of VapG was solved by molecular replacement with the program MOLREP (Vagin and Teplykov, 2010) using a family-related structure VapD (PDB code 4csb, Whittingham et al., 2014) as a search model, this sharing 60% amino acid sequence identity with VapG (Fig. 1B). Two solutions were found equating to two molecules of VapG per asymmetric unit. The resulting model was refined using maximum likelihood methods implemented in REFMAC5 (Murshudov et al., 2011) with 5% of the total data excluded from the refinement for the purpose of R free calculations. This procedure was interspersed with manual corrections to the model using COOT (Emsley et al., 2010) in conjunction with $2F_o - F_c$ and $F_o - F_c$ electron density maps.

During refinement, elongated peaks of positive difference electron density appeared in two independent locations in the asymmetric unit. These peaks had the appearance of additional protein chains or peptides bound between the protein molecules: in one location a sequence of three histidines was built and successfully refined; in the other the sequence ALAA was built. It was concluded that these elements formed parts of the C-terminal affinity tags from the two VapG molecules, with the ALAA corresponding to the tag sequence KLAA in one molecule and AALE in its symmetry mate. Another striking feature in the electron density maps was a strong metal ion peak located at the centre of a cluster of main chain and side chains oxygen donors from residues 107 to 114 of molecule A. The coordination distances ranged from 2.7 to 3.1 Å which was consistent with a potassium ion (Harding, 2002). Although other metal ion candidates (calcium and magnesium) were tested out in refinement, potassium was the only one which refined satisfactorily. Furthermore, X-ray absorption analysis of a single crystal revealed no other metal ions present apart from potassium, which was a crystallisation component. Refinement statistics and structural information are listed in Table 1.

2.4. Structure analysis

During analysis of the structure, multiple sequence alignment was performed using CLUSTAL-W (Thompson et al., 1994) and displayed using ESPript 3.0 (Robert and Gouet, 2014). Three dimensional structural alignments were made using secondary-structure matching (Krissinel and Henrick, 2004) implemented in COOT (Emsley et al., 2010). All figures were generated using CCP4mg (McNicholas et al., 2011).

Table 1
Crystallographic data collection and refinement statistics.

Data collection and processing statistics	
Diamond beamline/wavelength (Å)	I02/0.9795
Space group/cell dimensions (Å)	$P4_12_12/a = 44.6$, $c = 259.7$
Resolution limits (Å)[a]	31.50–1.80 (1.85–1.80)
No. unique reflections	24,979
Completeness (%)[a]	98.1 (83.4)
Multiplicity[a]	11.4 (7.2)
R_{merge}[a,b]	0.043 (0.674)
$I/\sigma I$[a]	31.4 (2.6)
Refinement statistics	
R_{cryst}[c]/R_{free}[d]	0.2009/0.2362
rmsΔ bond length (1–2) (Å)[e]	0.021 (0.019)
rmsΔ angles (°)[e]	1.893 (1.925)
rmsΔ chiral volumes (Å^3)[e]	0.126 (0.200)
Average *B* (Å^2): protein/waters and K+ ion	31.55/38.02
Ramachandran outliers (%)	0

[a] Highest resolution shell statistics given in parentheses.
[b] $R_{merge} = \sum_{hkl}\sum_i|I_i - \langle I\rangle|/\sum_{hkl}\sum_i\langle I\rangle$, where I_i is the intensity of the *i*th measurement of a reflection with indexes *hkl* and $\langle I\rangle$ is the statistically weighted average reflection intensity.
[c] $R_{cryst} = \sum||F_o| - |F_c||/\sum|F_o|$, where F_o and F_c are the observed and calculated structure factor amplitudes, respectively.
[d] *R*-free is the R_{cryst} calculated with 5% of the reflections chosen at random and omitted from refinement.
[e] Average geometric restraints given in parentheses.

Please cite this article in press as: Okoko, T., et al., Structural characterisation of the virulence-associated protein VapG from the horse pathogen *Rhodococcus equi*. Vet. Microbiol. (2015), http://dx.doi.org/10.1016/j.vetmic.2015.01.027

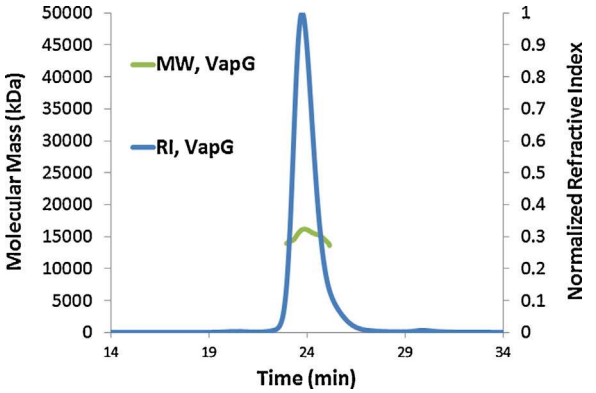

Fig. 2. Size exclusion chromatography with multi-angle laser light scattering (SEC-MALLS) analysis of VapG. The refractive index (RI) of the eluate from a Superdex S75 column is plotted as a function of time (blue trace). Over the peak region, the molecular weight (MW) of the species (green line) in the eluate is calculated from the light scattering measurements (For interpretation of the colour information in this figure legend, the reader is referred to the web version of the article.).

3. Results

3.1. Characterisation of recombinant VapG

The purified recombinant VapG protein was analysed by size exclusion chromatography with multi-angle laser light scattering. Here the protein is fractionated on a gel filtration column and the absorbance at 280 nm and the refractive index of the eluate are monitored together with the multi-angle light scattering of the sample. This enables the weight average molecular weight (M_w) of the eluting protein to be calculated continuously. The data from this experiment are shown in Fig. 2. Applying this analysis, we determined a molecular mass of 15.2 kDa for mature VapG fused to a C-terminal LEHHHHHH sequence. This compares with the mass calculated from the amino acid sequence of 16.0 kDa. It is clear therefore that VapG is a monomer.

3.2. Crystal structure of VapG

The recombinant protein used to obtain crystals comprised the mature VapG polypeptide (Fig. 1B) fused to a 20-residue sequence (PNSSSVDKLAAALEHHHHHH) at the C-terminus of the protein which included a poly-histidine affinity tag. As described earlier, the extended fusion portion of the protein formed intermolecular contacts critical for crystal growth. The asymmetric unit of the crystal contained two independent VapG molecules (molecules A and B). The refined structure consists of residues 42–147 of chain A and 41–147 of chain B. The low complexity N-terminal regions (residues up to and including Asn^{41} of chain A, and Ala^{40} of chain B) were not visible in the electron density maps. These residues were assumed, therefore, to be disordered. The same is true for most of the C-terminal tags (residues Asn^{148}-His^{166}) though short segments at the centre of these sequences were visible, mediating lattice contacts.

The A and the B molecules are virtually identical in fold. Following superposition of the two chains by least squares methods, the root mean squared deviation (rmsΔ) in corresponding C_α atom positions is 0.45 Å. Each molecule consists of eight β-strands and a single α-helix. The strands assemble to form a compact, anti-parallel β-barrel, which is elliptical in cross section (Fig. 3), and which has a β1–β2–β3–β8–β5–β6–β7–β4 topology. The N- and C-termini are each at the lower end of the barrel when it is viewed as in Fig. 3A and B. Thus β-turns link strands which are adjacent in the barrel; β1 and β2, and β5 and β6, at the top of the molecule and β2 and β3, and β6 and β7, at the base of the molecule. The remaining inter-strand connections, β3–β4 and β7–β8 at the top of the molecule (Fig. 3C) and β4–β5 at the base (Fig. 3D) cross-over the barrel effectively acting as caps that close off its ends. The β4–β5 connector contains the nine-residue α-helix. The short turns between strands and their close packing give the upper end of the molecule a smooth rounded surface, compared to the base where the β2–β3 and β6–β7 turns protrude outwards from the molecule to accommodate the α-helix.

The VapG protein fold described here was observed earlier for VapB and VapD and can be described as consisting of two Greek-key motifs separated by a small α-helix (Geerds et al., 2014; Whittingham et al., 2014). Despite the numerous occurrences of eight stranded β-barrel structures in the protein data bank (www.ebi.ac.uk/pdbe), the β1–β2–β3–β8–β5–β6–β7–β4 topology has not been observed elsewhere and it appears, therefore, that the Vap proteins are the defining members of a novel fold family.

Another interesting surface feature of the protein is a potassium ion which is bound at the head of the loop between β-strands 5 and 6 in molecule A (Fig. 4). The ion has a distorted octahedral coordination sphere consisting of the side chain oxygen atoms of residues Asn^{106} and Asn^{113} (both conserved), the main chain oxygen atoms of three residues Asn^{106}, Val^{108} and Tyr^{111} and a water molecule (Fig. 4). The equivalent site in molecule B does not contain a potassium ion as this site is occluded by the side chain of Ile^{76} of molecule A, which forms a crystal contact. This tight packing arrangement appears to be the cause of minor chain distortions in this loop in molecule B compared to molecule A.

3.3. The protein core

The core of VapG consists of densely packed, hydrophobic side chains many of which are contributed by alternate residues of the β-strands (Fig. 5A). A series of conserved aromatic side chains form an internal ladder that dominates one half of the protein core. Notable among the conserved residues is Trp^{145}, which is at the heart of the protein core and surrounded by side chains of Leu^{60}, Val^{62}, Phe^{69}, Leu^{88}, Leu^{96}, Tyr^{97} and Phe^{116} emanating from six different elements of secondary structure including the α-helix to which Trp^{145} makes extensive contacts. Curiously, the opposing half of the core is dominated by aliphatic side chains and devoid of aromatic groups (Fig. 5A). Evidently, this arrangement facilitates close packing in the protein interior and presumably enhances the stability of the barrel.

Please cite this article in press as: Okoko, T., et al., Structural characterisation of the virulence-associated protein VapG from the horse pathogen *Rhodococcus equi*. Vet. Microbiol. (2015), http://dx.doi.org/10.1016/j.vetmic.2015.01.027

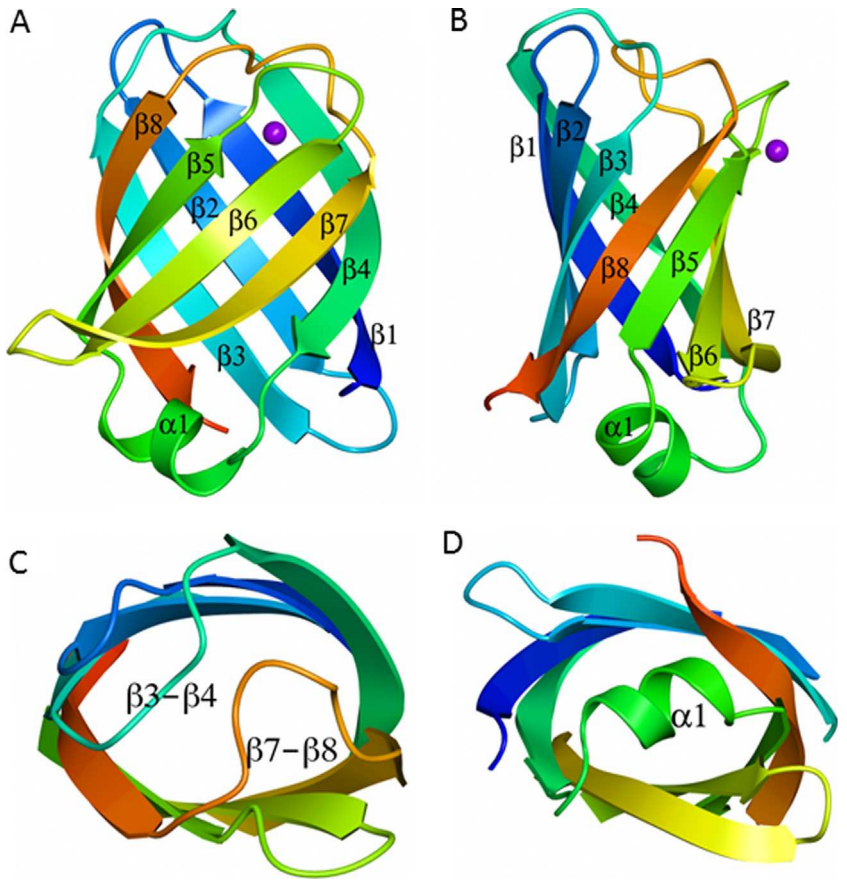

Fig. 3. The chain topology in VapG. (A) and (B) Approximately orthogonal views of the VapG chain represented as a ribbon trace colour-ramped from the N-terminus (blue) to the C-terminus (red). The secondary structure elements are labelled and the potassium ion from the A chain is shown as a purple sphere. (C) and (D) The VapG molecule coloured as above viewed parallel to the long axis of the barrel. It is apparent that the barrel is closed off by the β3–β4 and β7–β8 segments when viewed from above (C) and by the α1 helix when viewed from below (D). In (C) the potassium ion has been omitted for clarity (For interpretation of the colour information in this figure legend, the reader is referred to the web version of the article.).

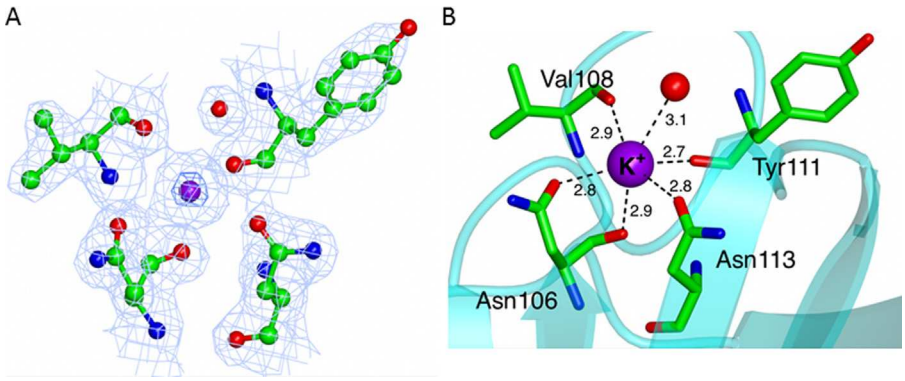

Fig. 4. Potassium coordination in the A molecule of VapG. (A) Electron density ($2F_{obs} - F_{calc}$) contoured at the 1σ and 6σ levels and displayed on the potassium ion, shown as a purple sphere, and neighbouring residues shown in ball-and-stick representation and coloured by atom type (carbon, green; nitrogen, blue; oxygen, red). (B) The bound potassium ion (K^+) is shown as a purple sphere with residues which contribute ligands to the metal centre shown in cylinder representation and with metal–ligand bonds shown as dashed lines. The bond lengths in Å are given.

The indole >NH of Trp^{145} forms a hydrogen bond to the hydroxyl of Thr^{100}, the only polar interaction in this region of the protein core. In the upper region of the core, the amide of the Gln^{56} side chain is at the centre of a local network of hydrogen bonds involving Ser^{73}, Ser^{77}, Tyr^{105} and a partially buried water molecule. The Gln^{56} to Tyr^{105} interaction, which links strands 2 and 5 is conserved in VapB and VapD and presumably VapA, although it is

Please cite this article in press as: Okoko, T., et al., Structural characterisation of the virulence-associated protein VapG from the horse pathogen *Rhodococcus equi*. Vet. Microbiol. (2015), http://dx.doi.org/10.1016/j.vetmic.2015.01.027

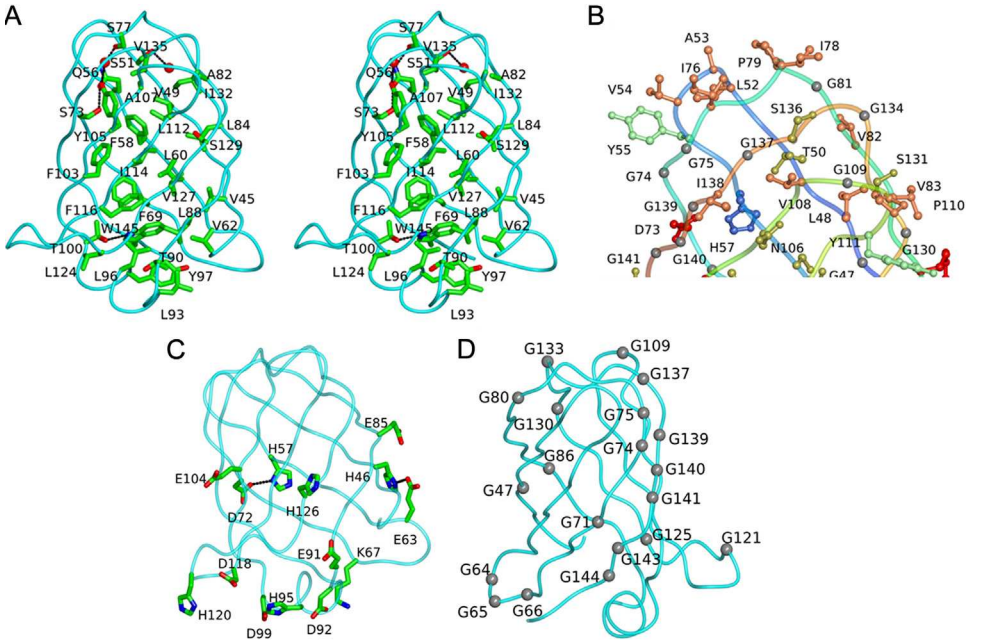

Fig. 5. Details of the structure of VapG. (A) Stereo view of the core of VapG. The protein backbone is represented as a worm tracing coloured in cyan and the side chains of residues that are significantly buried in the protein interior are shown in cylinder format and coloured by atom type (carbon, green; nitrogen, blue; oxygen, red). Two buried water molecules are shown as red spheres. Hydrogen bonding interactions between the buried side chains and these waters are shown as dashed lines. (B) The largely hydrophobic distal surface of VapG. The protein backbone is represented as a worm tracing colour ramped as in Fig. 3. Residues whose side chains are directed towards the solvent are shown in ball-and-stick representation and coloured according to their side chain type: non-polar aliphatic (Ala, Pro, Val, Leu, Ile), coral; aromatic (Trp, Tyr, Phe), light green; polar (Ser, Thr, Asn, Gln), gold; acidic (Glu, Asp) red; histidine, light blue. The Cα atoms of glycine residues are shown as grey spheres. (C) The distribution of ionisable residues in VapG. The side chains of acidic and basic residues are shown in cylinder format. (D) The distribution of the 20 glycine residues in VapG. The Cα atom of each glycine residue is shown as a grey sphere (For interpretation of the colour information in this figure legend, the reader is referred to the web version of the article.).

unlikely to be present in VapC or VapH (Fig. 1B). There is a second buried water which is hydrogen bonded to the side chain of Ser^{51} (Fig. 5A) and the main chain of residues Val^{49} and Thr^{134}.

3.4. The protein surface

The distribution of ionisable, polar and apolar groups on the surface of VapG is noticeably uneven (Fig. 5B and C). The upper third of the molecule viewed as in Fig. 5, is devoid of ionisable groups and the hydroxyl groups of Ser^{131}, Ser^{136}, Thr^{50} and Tyr^{55} represent the only polar side chain functional groups on this surface (Fig. 5B). Instead, the surface is dominated by exposed apolar side chains which give rise to an expansive hydrophobic surface area (Figs. 5B and 6C) which is extended by several conserved glycine residues which give this surface a flat as well as a neutral character. The lower reaches of the molecule on the other hand are significantly more polar. Seven of the 14 ionisable groups are located on or surrounding the α-helix at the base of the molecule while the remainder is located on a belt around the centre of the barrel (Fig. 5C).

The virulence-associated proteins are rich in glycine residues and the β-barrel domain of VapG contains 20 glycines in its 103 residues (Fig. 1B). This compares with the frequency of 7.4% for the occurrence of glycine residues in proteins as a whole. The distribution of these glycine residues is shown in Fig. 5D. The absence of a side chain in glycine is associated with main chain conformational flexibility and a proportion of these residues most notably Gly^{64}-Gly^{65}-Gly^{66} facilitate sharp turns between the secondary structure elements in the VapG protein chain. Others such as the striking cluster of Gly^{74}-Gly^{75} and Gly^{137} to Gly^{139}-Gly^{140}-Gly^{41} on strands β3 and β8, respectively, combine to create a flat and rather featureless protein surface. At many of the glycine positions, the side chain R groups of a non-glycine residue would be inward-facing and the presence of a Cβ atom would be expected to disrupt the close packing in the protein core. Thus for example, the glycines at positions 137, 139, 141 and 143 allow strand β8 to pack closely over the 'aromatic ladder' with the polypeptide segment 136–144 making no contribution to the protein core.

Table 2
Comparison of Vap protein sequences and structures. The table shows the pairwise percentage sequence identities over the β-barrel regions of the Vap proteins (light grey shading) and the rmsΔ in Cα coordinate positions deduced from the crystal structures (darker grey shading). For the VapG structure, the comparisons refer to molecule A.

	VapB	VapD	VapG
VapB	-	56	57
VapD	0.94	-	61
VapG	0.96	1.25	-

Please cite this article in press as: Okoko, T., et al., Structural characterisation of the virulence-associated protein VapG from the horse pathogen *Rhodococcus equi*. Vet. Microbiol. (2015), http://dx.doi.org/10.1016/j.vetmic.2015.01.027

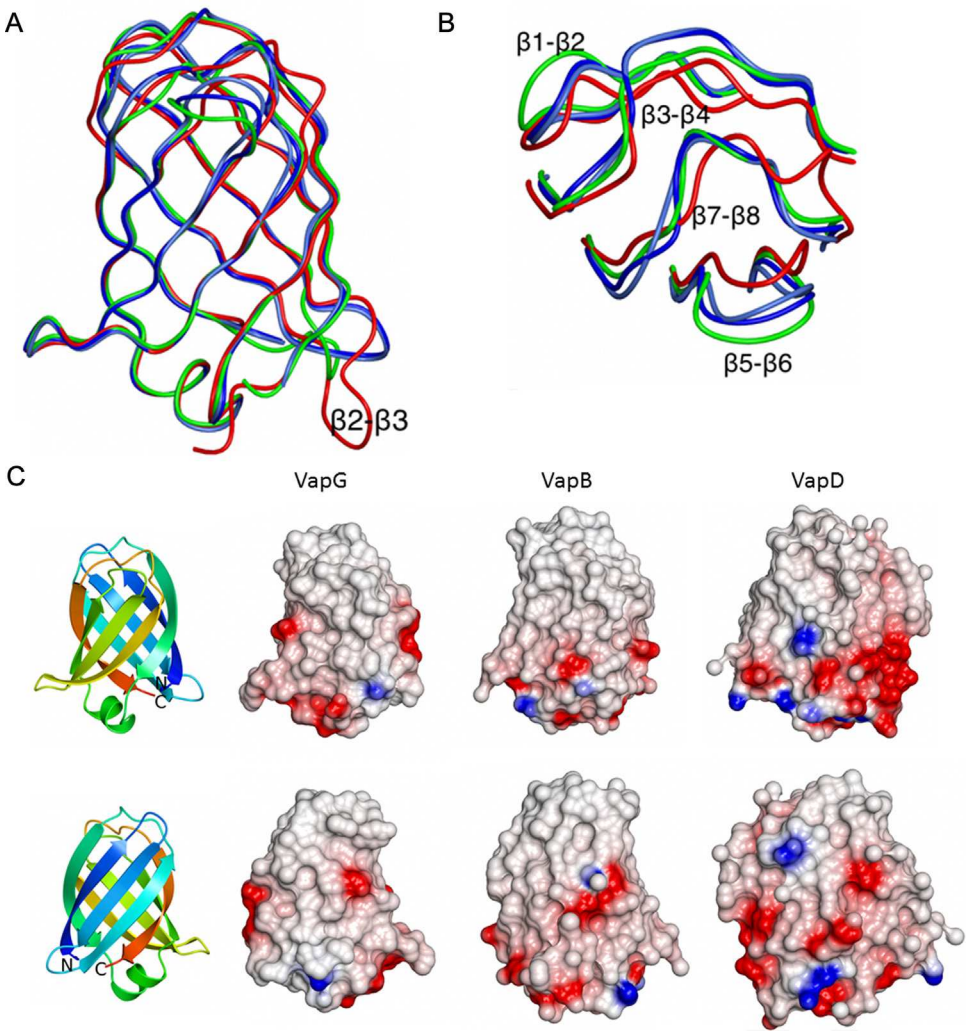

Fig. 6. Comparison of the crystal structures of the three *R. equi* virulence-associated proteins. (A) and (B) The structures of VapG molecule A (blue), VapG molecule B (light blue) VapD (red) and VapB (green) were overlaid using the SSM superpose routines in CCP4mg and the polypeptide backbones displayed as worm tracings. The superposed protein chains are viewed from the side illustrating the whole molecules (A) and from above parallel to the long axis of the barrel with the molecule clipped for clarity (B). (C) Electrostatic surface renderings of VapB, VapD and VapG with positive electrostatic potential in blue and negative electrostatic potential in red. The three molecules are viewed in two orientations which are illustrated by the ribbon tracing for VapG at the left. The extended apolar surface previously noted for VapD and VapB is evident (For interpretation of the colour information in this figure legend, the reader is referred to the web version of the article.).

3.5. Structure comparisons with VapB and VapD

The structures of VapB, VapD and the two molecules of VapG are compared in Table 2 and Fig. 6 (Geerds et al., 2014; Whittingham et al., 2014). The A and B molecules of VapG in the crystallographic asymmetric unit, coloured in different shades of blue, superpose more closely than either does onto VapB or VapD. Nevertheless, VapB, VapD and VapG share the same fold and are closely superimposable. It is apparent that VapB is more similar to VapD and VapG (lower pairwise rmsΔ values) than the latter pair is to each other, presumably reflecting the extent of sequence identity (Table 2). The molecules superimpose most closely in their central waist when viewed as in Fig. 6A, where the segments of structure form β-strands, and in the lower third of the structure where the only significant difference in structure is the β2–β3 loop where VapD and VapG contain one and five more residues than VapB, respectively. Otherwise, such differences as exist between pairs of structures are located in the loops at the opposite end of the molecule and these are apparent in Fig. 6B. One source of difference among the structures is the aspartic acid residue at the beginning of strand β4 in VapD (Whittingham et al., 2014). This residue plays an important role in determining the conformation of the β7–β8 loop in this protein by forming charge–dipole interactions with main chain amides from four consecutive residues in this loop. These interactions distort the conformation of the β7–β8 loop away from that which obtains in VapB and VapG. In VapB and VapG, the aspartate is replaced by smaller apolar residues, Gly and Ala, respectively, which allow the closer approach of the

Please cite this article in press as: Okoko, T., et al., Structural characterisation of the virulence-associated protein VapG from the horse pathogen *Rhodococcus equi*. Vet. Microbiol. (2015), http://dx.doi.org/10.1016/j.vetmic.2015.01.027

β7–β8 loop. Elsewhere, the presence of Pro^{110} on the β5–β6 loop of VapG contributes to differences in the conformation of this loop relative to VapB and VapD where the corresponding residue is Thr.

As shown in Fig. 6C, all three Vap proteins exhibit an asymmetric distribution of ionisable/polar residues and there is an amphipathic character to the molecules along the axis of the barrel. The base of all three molecules is richer in areas of both positive and negative electrostatic potential while there is an extended apolar surface over the dome at the top of the molecule (Geerds et al., 2014; Whittingham et al., 2014).

4. Discussion

The virulence plasmid of *R. equi* has long been recognised for its association with disease caused by this bacterium and VapA has emerged as a primary plasmid-encoded virulence determinant. VapA is the defining member of a family of proteins related by sequence and which are encoded in multiple copies by three types of virulence plasmid in *R. equi*, pVAPA which is primarily associated with disease in horses, pVAPB which is primarily associated with disease in pigs and pVAPN which is primarily associated with bovine isolates (Vázquez-Boland et al., 2013). *vap*-family genes have also been discovered in other bacterial genomes where they occur in single copy. Here, they encode proteins that lack recognisable secretion signal peptides and their functions are unknown (Vázquez-Boland et al., 2013; Whittingham et al., 2014). As an immuno-dominant marker in infection and as an essential virulence factor in *R. equi* disease in horses, VapA has been a focus of research in this field. Despite these efforts, relatively little is known about the cellular role of VapA, its biochemical activity, and its functional relationship, if any, to the five plasmid-encoded orthologues.

The structure of VapG determined in this work, complements those of VapB and VapD determined previously (Geerds et al., 2014; Whittingham et al., 2014). The close similarity of the three structures is no surprise given the high sequence identity and we can predict with confidence that the eight-stranded β-barrel occurs in the other Vap proteins including VapA. In each of the Vap proteins, the β-barrel domain is preceded by a 25–65 residue amino terminal peptide of variable sequence that is predicted to be natively disordered. Consistent with this prediction, in the crystals of VapG and VapD, the amino terminal region is present but not defined in the electron density maps indicating static or dynamic disorder in the crystals.

So what then are the functional implications of the crystal structures? An inspection of the surfaces of VapG, VapB and VapD reveals no significant depressions to indicate the presence of a ligand-binding cavity or an enzyme active site. Eight stranded barrel proteins with partial similarity to the Vaps occur elsewhere in bacterial cell surface/periplasmic proteins with roles in virulence. For example, bradavidin from *Bradyrhizobium japonicum* and PliC from *Salmonella typhimurium* function as a biotin binding protein and a periplasmic lysozyme inhibitor respectively (Leppiniemi et al., 2013; Leysen et al., 2011). In both instances, the proteins have an anti-parallel all-next-neighbour β-barrel topology β1–β2–β3–β4–β5–β6–β7–β8. The absence of crossover strands lends these barrels intrinsically more open structures, allowing one end of the barrel to develop as a binding/active site with the barrel interior forming the base of a ligand-binding cavity. There is less potential for a binding site in the Vap proteins due to the altered topology which leads to segments (β3–β4 and β7–β8) crossing over, and closing off, the top of the barrel (Fig. 3). At the opposing end, the barrel is closed off by the α-helix.

Similarly, the barrel domains of VapB, VapD and VapG have no obvious depressions or ridges on the protein surface to suggest protein interaction sites. This does not exclude the possibility that the Vaps are involved in interactions with other proteins since protein–protein recognition surfaces are variable in character (Janin et al., 2008). Moreover, such interactions may be mediated by the natively unfolded amino terminal regions and accompanied by a disorder-to-order transition upon interaction with a cognate bacterial or host factor. Alternatively, it is possible that VapA and the other Vap proteins have functions, which are manifested following a conformational change in the protein. Conformational changes frequently accompany the binding of small molecules to proteins. For example, in the starvation sensor CodY of *B. subtilis*, the branched chain amino acid binding site is absent in the crystal structure of the unliganded protein, its formation in the presence of ligand is accompanied by a large spontaneous rearrangement of loops elaborated from a β-sheet (Levdikov et al., 2009). Virulence factors in other pathogens undergo pH-dependent conformational changes. Indeed conformational changes in proteins associated with the phagolysosome pathway are amongst the largest to have been characterised by biophysical methods and observed/inferred from crystal structures (Bullough et al., 1994; Santelli et al., 2004). One example is the protective antigen (PA) of *Bacillus anthracis*, the cell entry component of the two-component toxins secreted by the anthrax causing bacterium. Following receptor binding on the host cell surface, PA assembles to form a heptameric prepore that binds the partner toxin, lethal factor or oedema factor, before being taken into the cell by endocytosis. The lowering of the pH upon endosome maturation, leads to protonation of a cluster of histidine residues on PA (Santelli et al., 2004) and rearrangement of a 75 residue largely disordered segment of the polypeptide to form an extended pair of β-strands linked by a β-turn. In the heptamer, the result is a 14-stranded β-barrel which forms a pore in the endosome membrane allowing the lethal and oedema factors to gain access to the host cell cytoplasm where they exert their toxic effects. In influenza virus, the surface protein haemagglutinin (HA), which is involved in cell surface binding and viral endocytosis, undergoes a dramatic conformational change upon acidification of the endosome (Bullough et al., 1994). Here, a cluster of aspartates becomes protonated as the pH is lowered allowing a random coil segment of HA to refold as an α-helix projecting the three amino terminal fusion peptides in the HA trimer 100 Å towards the endosome

Please cite this article in press as: Okoko, T., et al., Structural characterisation of the virulence-associated protein VapG from the horse pathogen *Rhodococcus equi*. Vet. Microbiol. (2015), http://dx.doi.org/10.1016/j.vetmic.2015.01.027

membrane where they facilitate fusion of the viral and endosome membranes and release of the viral contents into host cell cytoplasm.

The Vap proteins of *R. equi* do not have a role in endocytosis, instead they are secreted into the endosome by the phagocytosed bacterium and they have simpler structures than PA or HA. pH-induced activation of the Vap proteins, and VapA in particular, is appealing conceptually and *vap* gene expression is known to be induced in *R. equi* grown in equine macrophages and this induction can be mimicked by growth of bacteria at 37 °C at pH 5 under conditions of metal limitation (Ren and Prescott, 2003). However, a study of the maturation of *R. equi*-containing vesicles in mouse macrophages suggested many of the markers of the late endocytic stage were not acquired and there was arrest after completion of the early endosome stage (Fernandez-Mora et al., 2005). Specifically, the proton pumping ATPase was not acquired and the vesicles were not acidified. The prevailing view is that VapA has an upstream role in preventing acidification of the *R. equi*-containing vacuole and therefore is unlikely to be pH-activated.

A second question that may be posed concerns the determinants of the VapA sequence/structure responsible for its dominant role among the Vap proteins as a virulence factor in foals. Despite their similarities, the Vaps can be distinguished immunologically and it was reported that antibodies that recognise VapA do not cross react with recombinant Vaps C, D or E (Byrne et al., 2001). The sequence variability at the N-terminus of the Vap proteins has obvious potential for conferring differential function. Equally, it is established that proteins that have a common structural framework can perform diverse functions, thus, the limited sequence and structural differences in the β-barrel domains may allow the Vap proteins to make selective interactions. In relation to virulence, VapA may make interactions with a host factor that leads to a block in endosome maturation.

VapA is reported to be retained on the bacterial cell surface, and this localisation may be selective since VapC, VapD and VapE were shown to be secreted into the culture supernatants (Byrne et al., 2001). The cell surface presentation of VapA, perhaps as a complex with other bacterial factors or surface glycolipids, may be important in the virulence mechanism. It is also possible that the selective virulence properties of VapA are related to differential transcriptional regulation allowing the protein to attain a threshold concentration at a critical point in the life cycle of *R. equi* inside infected macrophages (Byrne et al., 2008).

5. Conclusion

The Vap proteins of *R. equi* consist of β-barrel domains with disordered regions at their N-termini. There are no intrinsic or comparative features of the Vap protein structures that provide clues to function. The structures provide a framework for structure-function studies of VapA but fuller understanding of *R. equi* virulence depends on the future identification of the interacting molecular partners of the Vap proteins.

Accession numbers

The atomic coordinates and structure factors have been deposited in the Protein Data Bank in Europe (www.ebi.ac.uk/pdbe) with the PDB ID code 5AEO.

Conflict of interest

None.

Acknowledgements

This work was supported by BBSRC Research Grant BB/J007900/1 to A.J.W. and the Tertiary Education Trust Fund (Nigeria) for T.O. We are grateful for access to the facilities at the Diamond Light Source. We are indebted to Johan Turkenburg, Eleanor Dodson, Andrew Leech and Sam Hart for technical assistance.

References

Andersen, S.J., Quan, S., Gowan, B., Dabbs, E.R., 1997. Monoxygenase-like sequence of a *Rhodococcus equi* gene conferring increased resistance to rifampin by inactivating this antibiotic. Antimicrobial Agents Chemother. 41, 218–221.

Asoh, N., Watanabe, H., Fines-Guyon, M., Watanabe, K., Oishi, K., Kositsakulchai, W., Sanchai, T., Kunsuikmengrai, K., Kahintapong, S., Khantawa, B., Tharavichitkul, P., Sirisanthana, T., Nagatake, T., 2003. Emergence of Rifampin-resistant *Rhodococcus equi* with several types of mutations in the *rhoB* gene among AIDS patients in northern Thailand. J. Clin. Microbiol. 2337–2340.

Benoit, S., Benachour, A., Taouji, S., Auffray, Y., Hartke, A., 2001. Induction of *vap* genes encoded by the virulence plasmid of *Rhodococcus equi* during acid tolerance response. Res. Microbiol. 152, 439–449.

Bullough, P.A., Hughson, F.M., Skehel, J.J., Wiley, D.C., 1994. Structure of influenza haemagglutinin at the pH of membrane fusion. Nature 371, 37–43.

Byrne, B.A., Prescott, J.F., Palmer, G.H., Takai, S., Nicholson, V.M., Alperin, D.C., Hines, S.A., 2001. Virulence plasmid of *Rhodococcus equi* contains inducible gene family encoding secreted proteins. Infect. Immun. 69, 650–656.

Byrne, G.A., Russell, D.A., Chen, X., Meijer, W.G., 2007. Transcriptional regulation of the virR operon of the intracellular pathogen *Rhodococcus equi*. J. Bacteriol. 189 (14), 5082–5089.

Byrne, G.A., Boland, C.A., O'Connell, E.P., Meijer, W.G., 2008. Differential mRNA stability of the vapAICD operon of the facultative intracellular pathogen *Rhodococcus equi*. FEMS Microbiol. Lett. 280, 89–94.

Colledge, V.L., Fogg, M.J., Levdikov, V.M., Leech, A., Dodson, E.J., Wilkinson, A.J., 2011. Structure and organisation of SinR, the master regulator of biofilm formation in *Bacillus subtilis*. J. Mol. Biol. 411, 597–613.

Coulson, G.B., Agarwal, S., Hondalus, M.K., 2010. Characterization of the role of the pathogenicity island and vapG in the virulence of the intracellular actinomycete pathogen *Rhodococcus equi*. Infect. Immun. 78, 3323–3334.

Dawson, T.R.M.Y., Horohov, D.W., Meijer, W.G., Muscatello, G., 2010. Current understanding of the equine immune response to *Rhodococcus equi*. An immunological review of *R. equi* pneumonia. Vet. Immun. Immunopathol. 135, 1–11.

Emsley, P., Lohkamp, B., Scott, W.G., Cowtan, K., 2010. Features and development of Coot. Acta Cryst. D66, 486–501.

Evans, P.R., 2011. An introduction to data reduction: space-group determination, scaling and intensity statistics. Acta Cryst. D67, 282–292.

Fernandez-Mora, E., Polidori, A., Lührmann, A., Schaible, U.E., Haas, A., 2005. Maturation of *Rhodococcus equi*-containing vacuoles is arrested after completion of the early endosome stage. Traffic 6, 635–653.

Geerds, C., Wohlmann, J., Haas, A., Niemann, H.H., 2014. Structure of *Rhodococcus equi* virulence-associated protein B (VapB) releals an eight-stranded antiparallel β-barrel consisting of two Greek-key motifs. Acta Cryst. F70, 866–871.

Giguère, S., Hondalus, M.K., Yager, J.A., Darrah, P., Mosser, D.M., Prescott, J.F., 1999. Role of the 85-kilobase plasmid and plasmid-encoded Virulence-associated protein A in intracellular survival and virulence of *Rhodococcus equi*. Infect. Immun. 67, 3548–3557.

Please cite this article in press as: Okoko, T., et al., Structural characterisation of the virulence-associated protein VapG from the horse pathogen *Rhodococcus equi*. Vet. Microbiol. (2015), http://dx.doi.org/10.1016/j.vetmic.2015.01.027

Giguère, S., Cohen, N.D., Chaffin, M.K., Slovis, N.M., Hondalus, M.K., Hines, S.A., Prescott, J.F., 2011. Diagnosis, treatment, control, and prevention of infections caused by *Rhodococcus equi* in foals. J. Vet. Intern. Med. 25, 1209–1220.

Harding, H.H., 2002. Metal-ligand geometry relevant to proteins and in proteins: sodium and potassium. Acta Cryst. D58, 872–874.

Hondalus, M.K., Mosser, D.M., 1994. Survival and replication of *Rhodococcus equi* in macrophages. Infect. Immun. 62, 4167–4175.

Hooper-McGrevy, K.E., Wilkie, B.N., Prescott, J.F., 2005. Virulence-associated protein-specific serum immunoglobulin G-isotype expression in young foals protected against *Rhodococcus equi* pneumonia by oral immunization with virulent *R. equi*. Vaccine 23, 5760–5767.

Jain, S., Bloom, B.R., Hondalus, M.K., 2003. Deletion of *vapA* encoding Virulence associated protein A attenuates the intracellular actinomycete *Rhodococcus equi*. Mol. Microbiol. 50, 115–128.

Janin, J., Bahadurm, R.P., Chakrabati, P., 2008. Protein–protein interaction and quaternary structur. Quart. Rev. Biophys. 41, 133–180.

Kabsch, W., 2010. XDS. Acta Cryst. D66, 125–132.

Kakuda, T., Hirota, T., Takeuchi, T., Hagiuda, H., Miyazaki, S., Takai, S., 2014. VirS, an OmpR/PhoB subfamily response regulator, is required for activation of vapA gene expression in *Rhodococcus equi*. BMC Microbiol. 14, 243.

Krissinel, E., Henrick, K., 2004. Secondary-structure matching (SSM), a new tool for fast protein structure alignment in three dimensions. Acta Cryst. D60, 2256–2268.

Leppiniemi, J., Meir, A., Kähkönen, N., Kukkurainen, S., Määttä, J., Ojanen, M., Jänis, J., Kulomaa, M., Livnah, O., Hytönen, V., 2013. The highly dynamic oligomeric structure of bradavidin II is unique among avidin proteins. Protein Sci. 22, 980–994.

Levdikov, V.M., Blagova, E., Colledge, V.L., Lebedev, A.A., Williamson, D.C., Sonenshein, A.L., Wilkinson, A.J., 2009. Structural rearrangement accompanying ligand binding in the GAF domain of CodY from *Bacillus subtilis*. J. Mol. Biol. 390, 1007–1018.

Leysen, S., Van Herreweghe, J., Callewaert, L., Heirbaut, M., Buntinx, P., Michiels, C., Strelkov, S., 2011. Molecular basis of bacterial defense against host lysozymes: X-ray structures of periplasmic lysozyme inhibitors PliI and PliC. J. Mol. Biol. 405, 1233–1245.

McNicholas, S., Potterton, E., Wilson, K.S., Noble, M.E.M., 2011. Presenting your structure: the CCP4mg molecular graphics software. Acta Cryst. D67, 386–394.

Meijer, W.G., Prescott, J.F., 2004. *Rhodococcus equi*. Vet. Res. 35, 383–396.

Miranda-CasoLuengo, R., Miranda-CasoLuengo, A.A., O'Connell, E.P., Fahey, R.J., Boland, C.A., Vázquez-Boland, J.A., Meijer, W.G., 2011. The *vapA* co-expressed virulence plasmid gene *vcgB* (*orf10*) of the intracellular actinomycete *Rhodococcus equi*. Microbiology 157, 2357–2368.

Murshudov, G.N., Skubak, P., Lebedev, A.A., Pannu, N.S., Steiner, R.A., Nicholls, R.A., Winn, M.D., Long, F., Vagin, A.A., 2011. REFMAC5 for the refinement of macromolecular crystal structures. Acta Cryst. D67, 355–367.

Muscatello, G., Leadon, D.P., Klay, M., Ocampo-Sosa, A., Lewis, D.A., Fogarty, U., Buckley, T., Gilkerson, J.R., Meijer, W.G., Vazquez-Boland, J.A., 2007. Rhodococcus equi infection in foals: the science of rattles. Equi. Vet. J. 39, 470–478.

Prescott, J.F., 1991. *Rhodococcus equi*: an animal and human pathogen. Clin. Microbiol. Rev. 4, 20–34.

Ren, J., Prescott, J.F., 2003. Analysis of virulence plasmid gene expression of intra-macrophage in in vitro grown *Rhodococcus equi* ATCC33701. Vet. Microbiol. 94, 167–182.

Robert, X., Gouet, P., 2014. Deciphering key features in protein structures with the new ENDscript server. Nucl. Acid Res. 42 (W1), W320–W324, doi:10.1093/nar/gku316 (freely accessible on-line).

Russell, D.A., Byrne, G.A., O'Connell, E.P., Boland, C.A., Meijer, W.G., 2004. The LysR-type transcriptional regulator VirR is required for expression of the virulence gene *vapA* of *Rhodococcus equi* ATCC 33701. J. Bacteriol. 186, 5576–5584.

Santelli, E., Bankston, L.A., Leppla, S.H., Liddington, R.C., 2004. Crystal structure of a complex between anthrax toxin and its host cell receptor. Nature 430, 905–908.

Takai, S., Koike, K., Ohbushi, S., Izumi, C., Tsubaki, S., 1991a. Identification of 15- to 17- kilodalton antigens associated with virulent *Rhodococcus equi*. J. Clin. Microbiol. 29, 439–443.

Takai, S., Sekizaki, T., Ozawa, T., Sugawara, T., Watanabe, Y., Tsubaki, S., 1991b. Association between a large plasmid and 15- to 17-kilodalton antigens in virulent *Rhodococcus equi*. Infect. Immun. 59, 4056–4060.

Takai, S., Iie, M., Watanabe, Y., Tsubaki, S., Sekizaki, T., 1992. Virulence-associated 15- to 17-kilodalton antigens in *Rhodococcus equi*: temperature-dependent expression and location of the antigens. Infect. Immun. 60, 2995–2997.

Tan, C., Prescott, J.F., Patterson, M.C., Nicholson, V.M., 1995. Molecular characterization of a lipid-modified virulence-associated protein of *Rhodococcus equi* and its potential protective immunity. Can. J. Vet. Res. 59, 51–59.

Tkachuk-Saad, O., Prescott, J., 1991. *Rhodococcus equi* plasmids: isolation and partial characterization. J. Clin. Microbiol. 29, 2696–2700.

Thompson, J.D., Higgins, D.G., Gibson, T.J., 1994. CLUSTAL-W—improving the sensitivity of progressive multiple sequence alignment through sequence weighting, position-specific gap penalties and weight matrix choice. Nucl. Acid Res. 22, 4673–4680.

Vagin, A., Teplykov, A., 2010. Molecular replacement with MOLREP. Acta Cryst. D66, 22–25.

Vázquez-Boland, J.A., Giguère, S., Hapeshi, A., MacArthur, I., Anastasi, E., Valero-Rello, A., 2013. *Rhodococcus equi*: the many facets of a pathogenic actinomycete. Vet. Microbiol. 167, 9–33.

Wada, R., Kamada, M., Anzai, T., Nakanishi, A., Kanemaru, T., Takai, S., Tsubaki, S., 1997. Pathogenicity and virulence of *Rhodococcus equi* in foals following intratracheal challenge. Vet. Microbiol. 56, 301–312.

Whitehead, A.E., Parreira, V.R., Hewson, J., Watson, J.L., Prescott, J.F., 2012. Development of a live, attenuated, potential vaccine strain of *R. equi* expressing *vapA* and the *virR* operon, and virulence assessment in the mouse. Vet. Imm. Immunopathol. 145, 479–484.

Whittingham, J.L., Blagova, E.V., Finn, C.E., Luo, H., Miranda-CasoLuengo, R., Turkenburg, J.P., Leech, A.P., Walton, P.H., Murzin, A.G., Meijer, W.G., Wilkinson, A.J., 2014. Structure of the virulence-associated protein VapD from the intracellular pathogen *Rhodococcus equi*. Acta Cryst. D70, 2139–2151.

Please cite this article in press as: Okoko, T., et al., Structural characterisation of the virulence-associated protein VapG from the horse pathogen *Rhodococcus equi*. Vet. Microbiol. (2015), http://dx.doi.org/10.1016/j.vetmic.2015.01.027